Stewart et al., http://www.jcb.org/cgi/content/full/jcb.201502024/DC1

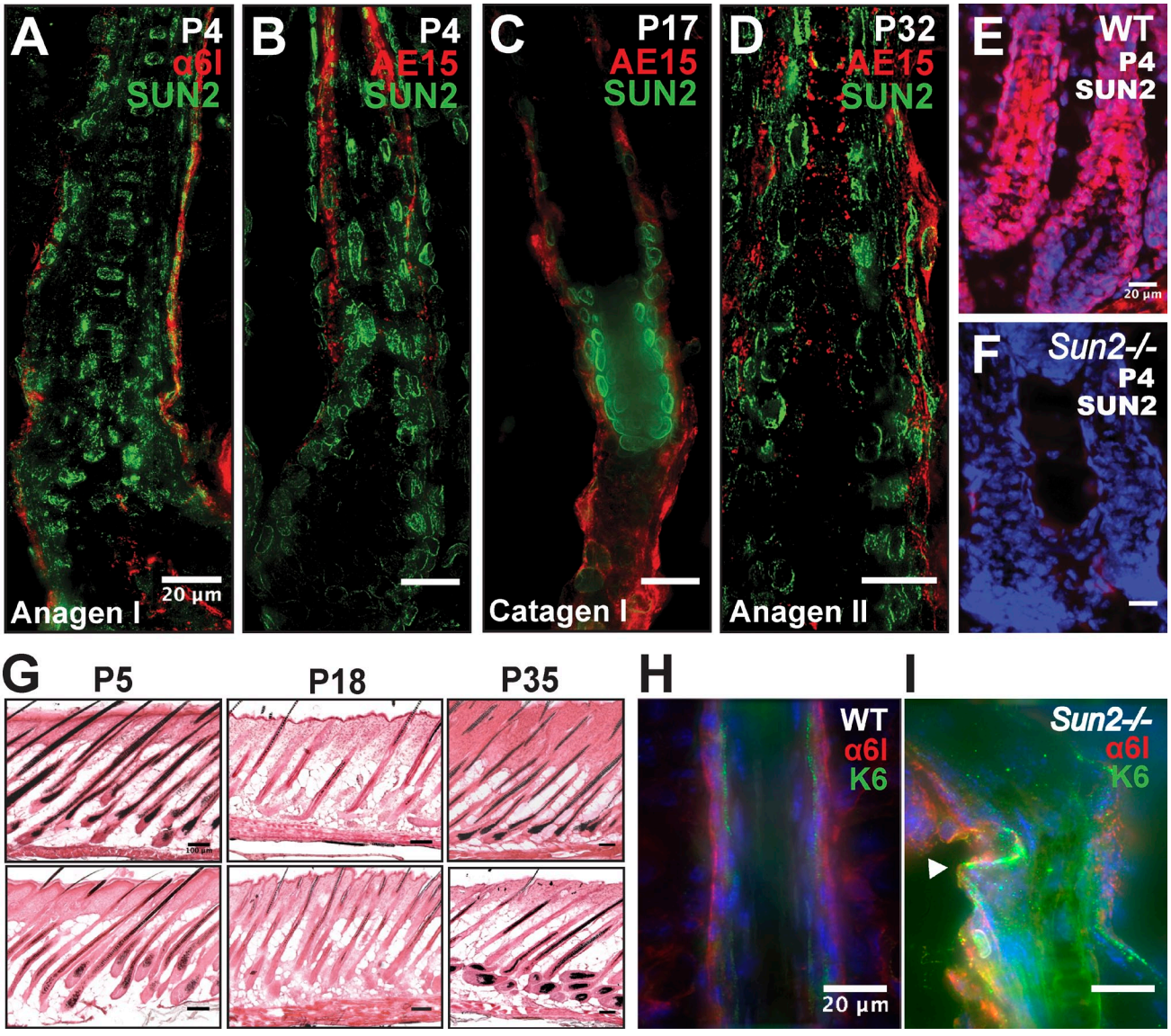

Figure S1. ***Sun1*$^{-/-}$ murine hair follicle morphology is not perturbed, but bends in *Sun2*$^{-/-}$ follicles extend through all layers of the follicle.** (A–D) Back skin from P4 WT mice showing localization of SUN2, α_6 integrin (α6I), and trichohyalin (AE15). SUN2 was expressed through all layers of the hair follicle at P4 and P32, including the ORS (α_6 integrin, in A) and IRS (AE15, in B–D). At P17, SUN2 was highly expressed in the cells surrounding the hair shaft as well as in the epithelial strand and upper regions of the follicle (C). (E and F) Back skin from P4 WT and *Sun2*$^{-/-}$ mice was sectioned, and immunostaining for SUN2 (red) revealed robust SUN2 staining in WT follicles and the absence of staining in *Sun2*$^{-/-}$ follicles. (G) Back skin from P5, P18, and P35 WT and *Sun1*$^{-/-}$ mice was sectioned and stained with hematoxylin and eosin. No differences in follicle morphology were observed between WT and *Sun1*$^{-/-}$ follicles. Bars, 100 µm. (H and I) Back skin from P4 WT and *Sun2*$^{-/-}$ mice was sectioned and immunostained for K6 and α_6-integrin. Bends in *Sun2*$^{-/-}$ follicles extended through the companion layer (K6) to the ORS (α_6-integrin). Arrowhead indicates a severe bend in in the *Sun2*$^{-/-}$ hair follicle that extends from the companion layer (K6) to the ORS (α_6-integrin).

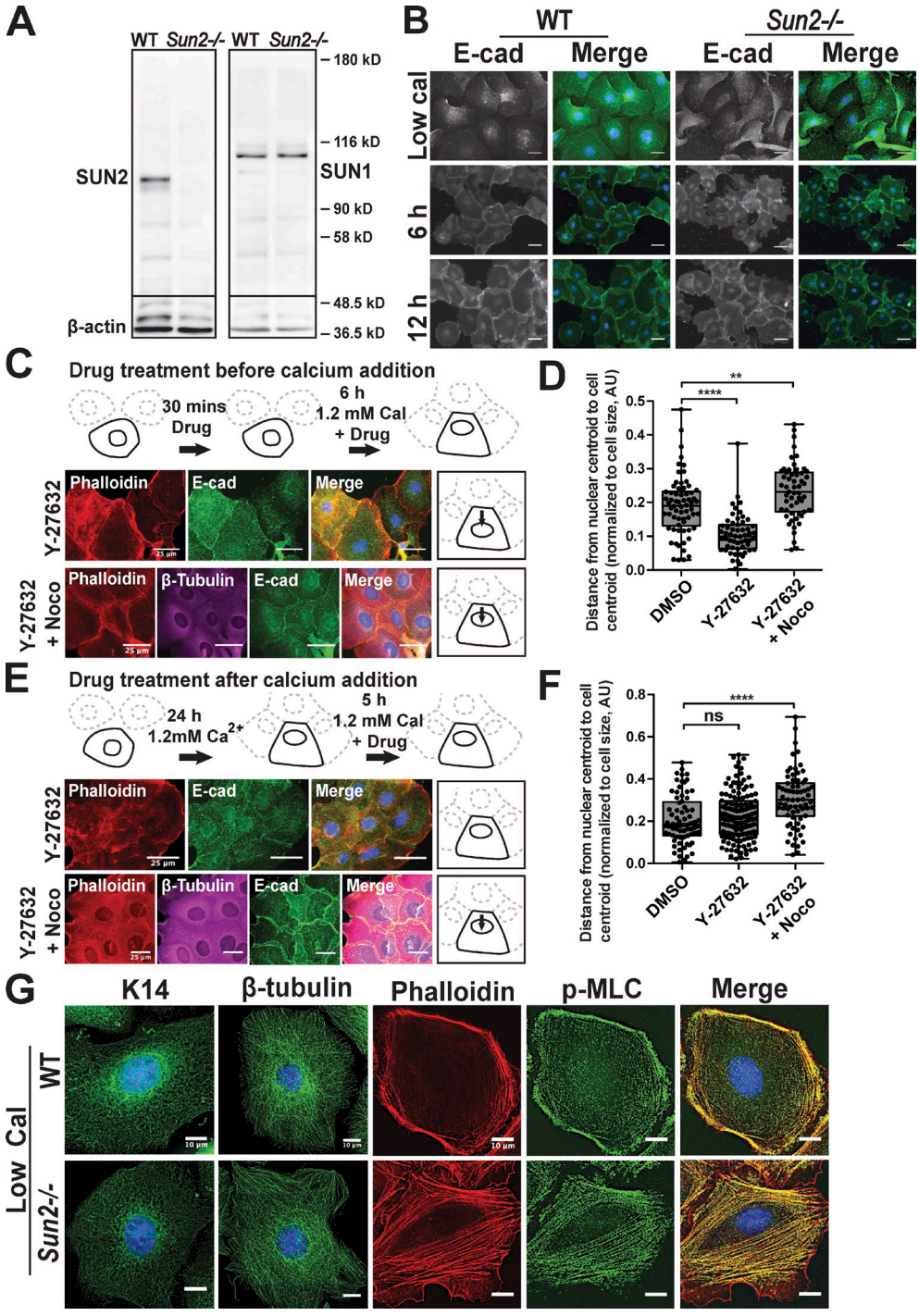

Figure S2. **Actin and MTs differentially regulate adhesion-dependent nuclear movement.** (A) Western blot analysis of whole-cell lysates from WT and *Sun2*$^{-/-}$ MKCs probed with antibodies against SUN2, SUN1, and β-actin (loading control). Black lines indicate that intervening lanes have been spliced out. (B) WT and *Sun2*$^{-/-}$ MKCs were cultured in high calcium medium for 0, 6, and 12 h and then immunostained for E-cad (green) and counterstained with Hoechst (nuclei, blue). Also see Fig. 2 (C–E). Bars, 50 µm. (C) Diagram illustrating the sequence of drug addition to WT MKCs before calcium addition. E-cadherin (E-cad), β-tubulin (magenta), actin (phalloidin, red), and nuclei (Hoechst, blue) localization are shown. Diagrams in B illustrate the effect of drug treatment on nuclear position relative to the DMSO-treated control (Fig. 3 B). (D) Plots of the nuclear centroid to cell centroid distance normalized to cell radius. Nuclei in Y-27632–treated cells did not move toward adhesions as they did in control cells and instead remained at the cell center. Like blebbistatin in combination with nocodazole (Fig. 3, B and D), Y-27632 also partially rescued the excessive nuclear movement observed in nocodazole-treated cells. $n > 50$ cells for all conditions (representative of three independent experiments). Asterisks denote indicated significance. (**, $P \leq 0.01$; ****, $P \leq 0.0001$; ANOVA with Dunnett's posttest). (E) Diagram illustrating the sequence of drug addition to WT MKCs after calcium addition. E-cad (green), β-tubulin (magenta), actin (phalloidin, red), and nuclei (Hoechst, blue) localization are shown. Diagrams in E illustrate the effect of drug treatment on nuclear position relative to the DMSO-treated control (Fig. 3 F). (F) Plots of the nuclear centroid to cell centroid distance normalized to radius. Nuclear position in Y-27632–treated cells did not differ from control cells (see also Fig. 3, F and G). Y-27632 in combination with nocodazole could partially rescue the excessive nuclear movement observed in nocodazole-treated cells (see also Fig. 3, F and H). $n > 50$ cells for all conditions (representative of three independent experiments). Asterisks denote indicated significance. (ns, not significant; ****, $P \leq 0.0001$; ANOVA with Dunnett's posttest). (G) WT and *Sun2*$^{-/-}$ MKCs cultured in low calcium medium were immunostained for β-tubulin (green), phosphorylated myosin light chain (p-MLC, green), keratin 14 (K14, green), and counterstained with phalloidin (actin, red) and Hoechst (nuclei, blue). Perinuclear K14 and β-tubulin cages are not observed in either WT or *Sun2*$^{-/-}$ cells, whereas excessive stress fibers are present in *Sun2*$^{-/-}$ cells. For box and whiskers plots, the bottom and top of the box display the 25th and 75th percentiles, whereas the central band represents the median. The whiskers indicate the minimum and maximum values, and the plus signs indicate the means. AU, arbitrary unit; Cal, calcium; Noco, nocodazole.

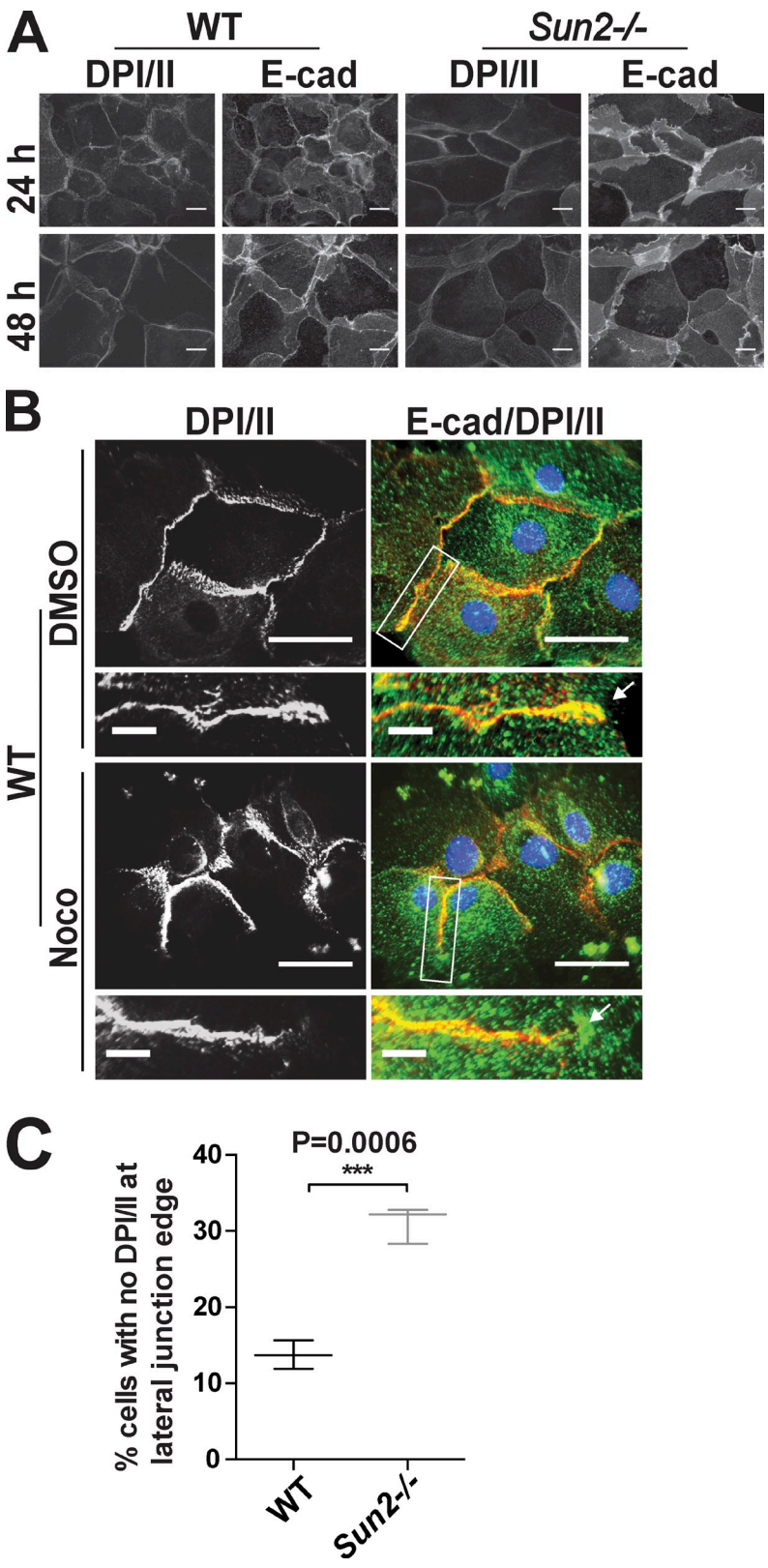

Figure S3. ***Sun2*$^{-/-}$ MKCs form intercellular adhesions but exhibit perturbed adhesion-dependent nuclear position and desmosome distribution.** (A) Induction of adhesion between WT or *Sun2*$^{-/-}$ MKCs in high calcium medium after 24 and 48 h revealed AJ (E-cad) and desmosome (DPI/II) formation. Also see Fig. 5 A. (B) WT MKCs cultured in low calcium medium were incubated with nocodazole or DMSO for 30 min followed by calcium for an additional 6 h. Immunostaining for DPI/II (red), E-cad (green), and Hoechst (nuclei, blue) revealed an even distribution of DPI/II along apical and lateral junctions in control cells, whereas DPI/II accumulated at interior junctions in nocodazole-treated cells. Although DPI/II extended out to lateral junction edges in control cells, DPI/II was depleted at the edges of these junctions in nocodazole-treated cells (arrows). See quantification in Fig. 5 F. (C) Quantification of the percentage of lateral junctions lacking DPI/II at the cell edge. *Sun2*$^{-/-}$ MKCs exhibited significantly fewer junctions with DPI/II at the cell edge than WT MKCs. $n > 150$ junctions from three independent experiments. Statistical significance determined by unpaired, two-tailed *t* test. See Fig. 5 (D and H). The whiskers in the graph indicate the minimum and maximum values, and the central band represents the median. Noco, nocodazole. Bars, 50 µm.

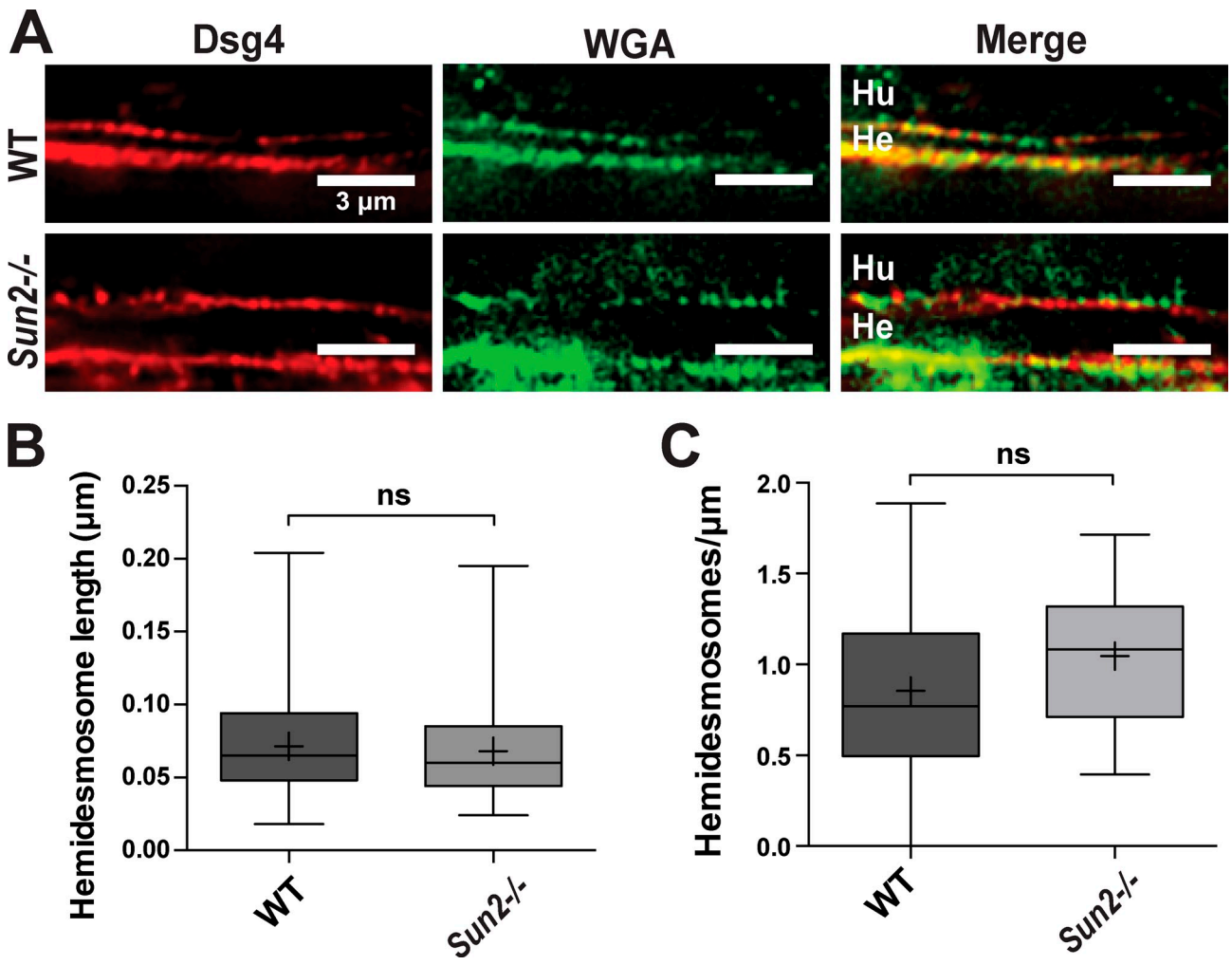

Figure S4. **Hemidesmosome morphology and number are not altered in *Sun2*$^{-/-}$ murine hair follicles.** (A) Back skin sections from P4 WT and *Sun2*$^{-/-}$ mice were fixed and immunostained for desmoglein 4 (Dsg4, red) and counterstained with fluorophore-conjugated WGA (green). Junctions between Henle (He) and Huxley (Hu) layer cells were identified by WGA staining, allowing fluorescence intensity measurements to be made (as in Fig. 6, K and L). (B) Quantification of hemidesmosome length in WT and *Sun2*$^{-/-}$ hair follicles from transmission electron micrographs. No differences in hemidesmosome morphology were observed in *Sun2*$^{-/-}$ follicles compared with WT follicles. WT $n = 74$ hemidesmosomes and *Sun2*$^{-/-}$ $n = 75$ hemidesmosomes from two mice. Statistical significance was determined by unpaired, two-tailed *t* test. (C) Quantification of hemidesmosome density between ORS cells and the basement membrane in WT and *Sun2*$^{-/-}$ hair follicles. No differences in hemidesmosome number were observed in *Sun2*$^{-/-}$ follicles compared with WT follicles. WT $n = 12$ cells and *Sun2*$^{-/-}$ $n = 12$ cells from two mice. ns, not significant. Statistical significance was determined by unpaired, two-tailed *t* test. For box and whiskers plots, the bottom and top of the box display the 25th and 75th percentiles, whereas the central band represents the median. The whiskers indicate the minimum and maximum values, and the plus signs indicate the means.

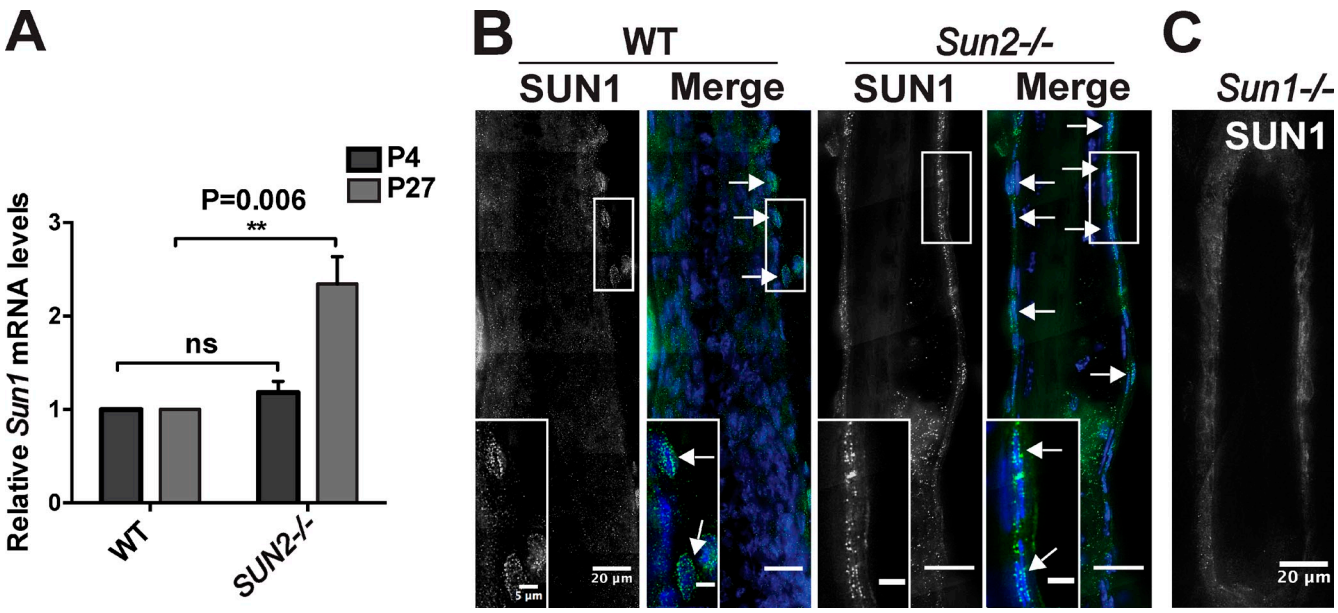

Figure S5. **Hair follicle structure recovers after the first hair cycle concomitant with up-regulation of SUN1.** (A) Real-time PCR analysis of *Sun1* mRNA gene expression in *Sun2*$^{-/-}$ or WT isolated hair follicles from P4–5 or P27 mice. Data shown represent mean values from three separate experiments using pairs of *Sun2*$^{-/-}$ or WT mice, presented as means ± SEM. (B) Frozen back skin from P32 WT and *Sun2*$^{-/-}$ mice was sectioned and immunostained with an antibody against SUN1 (green) and counterstained with Hoechst (nuclei, blue). Increased SUN1 expression, visualized as increased specific NE staining, was present at P32 in WT follicles, but more so in *Sun2*$^{-/-}$ follicles. Arrowheads indicate specific SUN1 staining. Boxes are enlarged in the insets. (C) Background nonspecific staining of the anti-SUN1 antibody as assessed by staining sections of frozen back skin from a P32 *Sun1*$^{-/-}$ mouse.